

# Uniform Temperature Cooling Power of the Superfluid Stirling Refrigerator

A. Watanabe,<sup>1</sup> G. W. Swift,<sup>2</sup> and J. G. Brisson<sup>1</sup>

<sup>1</sup>Cryogenic Engineering Laboratory, Massachusetts Institute of Technology,  
Cambridge, MA 02139, USA

<sup>2</sup>Condensed Matter and Thermal Physics Group, Los Alamos National Laboratory,  
Los Alamos, NM 87545, USA

(Received January 23, 1996; revised March 7, 1996)

*Uniform temperature cooling power measurements of a superfluid Stirling refrigerator are presented for  $^3\text{He}$ - $^4\text{He}$  molar concentrations of 5.9%, 17% and 36% and for temperatures between 0.37 K and 1.4 K. The results are compared to an ideal Fermi gas model and to a more general thermodynamic model. The Fermi model agrees well with the 5.9% concentration data; however, the more elaborate model is needed for higher concentration mixtures.*

## 1. INTRODUCTION

The superfluid Stirling refrigerator (SSR) is a relatively new type of sub-Kelvin refrigerator that uses a  $^3\text{He}$ - $^4\text{He}$  liquid mixture as the working fluid. The  $^3\text{He}$  component of the working fluid, to first approximation, behaves thermodynamically as an ideal gas in an inert background of superfluid  $^4\text{He}$ .<sup>1</sup> Using pistons equipped with a superleak bypass, it is possible to expand and compress the  $^3\text{He}$  solute "gas" alone. The SSR is a Stirling machine equipped with these "superleaked" pistons to use the properties of the  $^3\text{He}$  solute to cool below 1 K. The proof of principle was shown by Kotsubo and Swift in 1990.<sup>2,3</sup>

The principal components and the operation of the superfluid Stirling refrigerator can be understood by referring to Fig. 1. The  $^3\text{He}$ - $^4\text{He}$  mixture is held between two pistons, each bypassed by a superleak. Behind each of the pistons is a reservoir of pure  $^4\text{He}$ . Due to its superfluid nature below 2 K, the  $^4\text{He}$  in the reservoirs and in the  $^3\text{He}$ - $^4\text{He}$  mixture will freely pass through the piston superleaks as the pistons move. The  $^3\text{He}$ , which behaves as a normal fluid, is confined to the volume between the pistons.

The regenerator can be thought of as a large array of small diameter, high heat capacity tubes. In the ideal regenerator, the passages in the tubes have negligible volume and the longitudinal thermal conductivity of these tubes is zero. The regenerator has a longitudinal temperature gradient from

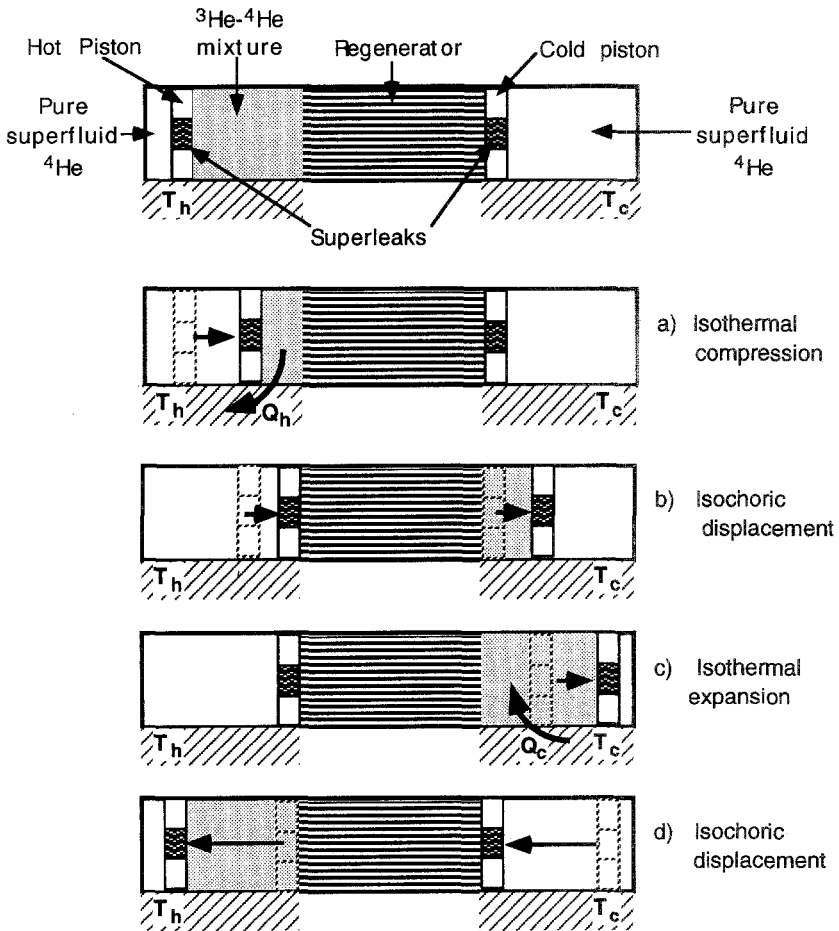


Fig. 1. The four steps in the operation of the superfluid Stirling refrigerator.

the hot piston to the cold piston chamber. Any fluid particle that migrates from the hot piston chamber to the cold piston chamber will reversibly exchange heat with the high heat capacity regenerator wall and emerge into the cold piston cavity at the cold piston temperature,  $T_c$ . Conversely, fluid particles that migrate through the regenerator from the cold piston to the hot piston will emerge at the hot piston temperature,  $T_h$ .

The ideal cycle starts with all the mixture in the hot piston chamber. The  $^3\text{He}$  in the mixture is compressed isothermally (Fig. 1a) as the hot piston is moved towards the regenerator. Because the  $^3\text{He}$  behaves as an ideal gas, heat is rejected to the thermal reservoir at  $T_h$ . Next, both pistons are moved in tandem so that the compressed fluid is displaced through the regenerator at constant total volume (Fig. 1b). In this process, the  $^3\text{He}$  releases heat to the regenerator matrix. The  $^3\text{He}$  component of the mixture is now in a low-temperature compressed state. The cold piston now moves to expand the  $^3\text{He}$  isothermally (Fig. 1c), absorbing heat from the low-temperature thermal reservoir. Following this expansion, both pistons move in tandem to pass the expanded  $^3\text{He}$  component back through the regenerator at constant total volume (Fig. 1d). In this process, the  $^3\text{He}$  reclaims the heat from the regenerator that it deposited there earlier. The refrigerator is now back in its original state and ready to start a new cycle.

In actuality, the  $^4\text{He}$  neutral atmosphere- $^3\text{He}$  ideal Boltzmann gas picture presented above is an oversimplification. For example, the low-concentration, high-temperature cooling power of the SSR can be significantly enhanced by the presence of phonons and rotons in the  $^4\text{He}$  component of the mixture.<sup>4</sup> Below, we will show that at low temperatures and low concentrations, the  $^3\text{He}$  component behaves as an ideal Fermi gas. At higher concentrations and temperatures, the thermodynamic properties of the working fluid are not characterized by either of these simple models.

We investigated SSR operation with high  $^3\text{He}$  concentrations since the cooling power of the SSR increases with increasing  $^3\text{He}$  concentration. In addition, we also investigated the low temperature operation of the SSR to observe the effect of the transition of the working fluid from a Boltzmann to a Fermi gas.

This refrigerator typically operates with the temperature ratio,  $T_h/T_c$ , equal to about three, but in the experiments described here, the SSR is operated at constant temperature in both time and space. This results in great simplification of the analysis and allows a straightforward comparison of the SSR performance to various thermodynamic models of the working fluid. The SSR performance measurements for non-uniform temperature distributions are discussed elsewhere.<sup>5</sup>

The next section discusses the experimental apparatus and procedure, followed by the experimental results. Section 3 is a review of the ideal

Fermi gas model and a derivation of the ratio of the cooling power to the cold piston work for a uniform temperature SSR operating with an ideal Fermi gas. Section 4 reviews the results of Brisson and Swift<sup>4</sup> which allows the comparison of the SSR performance to the thermodynamic tables of Radebaugh.<sup>6</sup> Finally, Sec. 5 discusses the differences between the models and the data.

## 2. MEASUREMENTS

The refrigerator used in this investigation, shown in Fig. 2, is actually two Stirling refrigerators operating  $180^\circ$  out of phase with each other. The

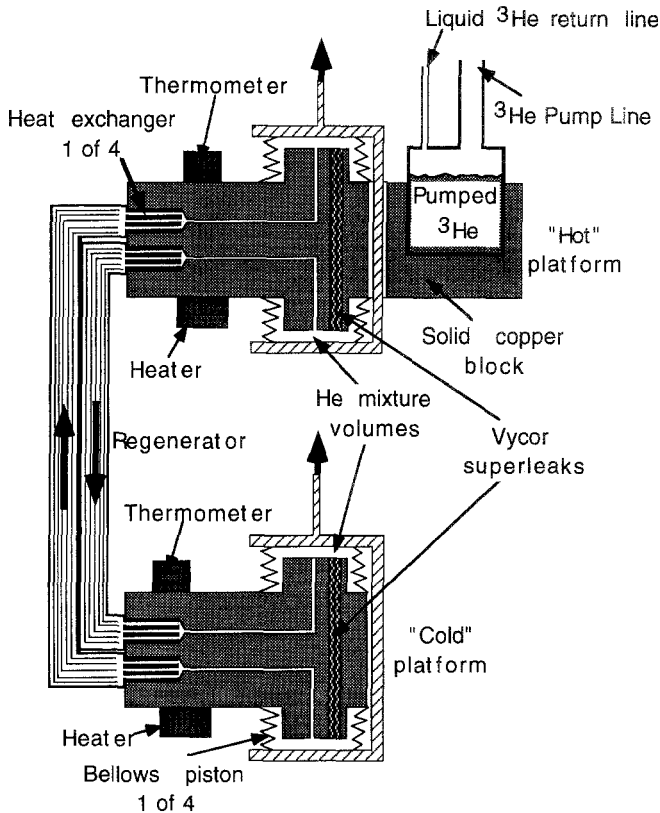


Fig. 2. The recuperative superfluid Stirling refrigerator used in this investigation. It consists of two Stirling refrigerators. The "hot" ("cold") pistons are ganged together so that the refrigerators operate  $180^\circ$  out of phase with each other. The pumped  $^3\text{He}$  pot removes the heat rejected by the SSR to the "hot" platform. The heavy arrows in the regenerator show the direction of fluid flow when the pistons are moved as indicated.

refrigerators reject heat to a “hot” platform that is cooled by a  $^3\text{He}$  evaporation refrigerator. This apparatus differs from the refrigerator shown in Fig. 1 in that the regenerator is a counterflow heat exchanger and that the pure  $^4\text{He}$  space has been replaced by the other Stirling refrigerator. In addition, the pistons in the actual refrigerator are driven sinusoidally and not in the articulated fashion discussed above.

The pistons are made using edge welded bellows.<sup>7</sup> The superleaks between the pistons are Vycor glass rods of diameter 3.6 mm and 7.4 cm long. The heat exchangers are copper cylinders press fit into the large copper blocks on which the pistons are mounted. The “hot” platform heat exchanger cylinders are 1.14 cm long with four 0.8 mm diameter holes drilled longitudinally through the cylinder. The “cold” platform heat exchanger cylinders are 1.14 cm long with twelve longitudinal 0.51 mm diameter holes.

The counterflow heat exchanger consists of a total of 238 0.305 mm O.D. CuNi tubes with 0.038 mm walls. These tubes are silver soldered in a hexagonally close packed array with alternating rows corresponding to each

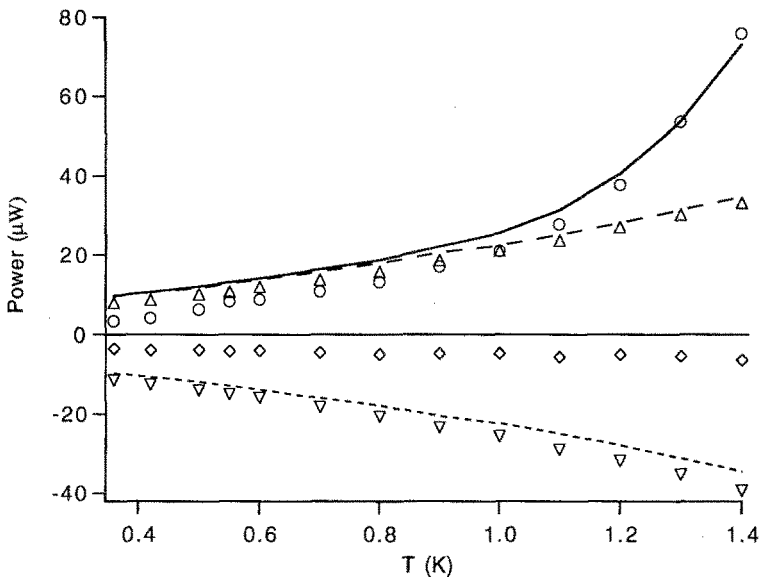


Fig. 3. Measured cooling power ○, hot piston work per unit time ▽, cold piston work per unit time △ and total piston work per unit time ◇ of the SSR under isothermal conditions as a function of temperature. The working fluid is a 5.9% molar mixture and the period of operation is 100 s. The pistons each sweep a volume of 0.78 cm<sup>3</sup>. The solid line and the long dashed line are, respectively, the calculated cooling power and the cold piston work per unit time using Eqs. 14 and 15 and Radebaugh's tables. The short dashed line is the calculated hot piston work per unit time.

“half” of the refrigerator. The length of the regenerator is approximately 20 cm.

Throughout these measurements, germanium resistance thermometers and feedback-controlled heaters were used to regulate the temperatures of both the “cold” platform and the hot platform to a common temperature. In these measurements, the common temperature,  $T$ , was varied from 0.37 K to 1.4 K. The power delivered to the cold platform heater is the cooling power of the refrigerator with zero temperature difference across the refrigerator.  $^3\text{He}$  molar concentrations of 5.9%, 17% and 36% were used in these measurements. These solutions were prepared by careful mixing of pure  $^3\text{He}$  and  $^4\text{He}$  gases, and their concentrations were checked by measuring the solution’s sound speed at  $0^\circ\text{C}$ . In these measurements, the total volume of  $^3\text{He}$ - $^4\text{He}$  mixture contained in both halves of the SSR is  $14.6\text{ cm}^3$ .

The operation of the refrigerator under spatially and temporally isothermal conditions provides an important simplification in the analysis of the refrigerator’s performance. Since there are no temperature gradients

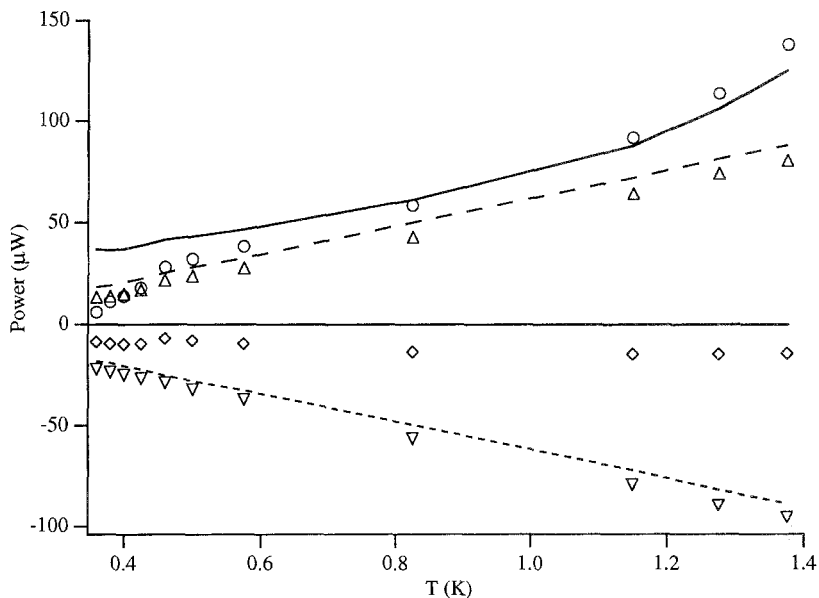


Fig. 4. Measured cooling power  $\circ$ , hot piston work per unit time  $\nabla$ , cold piston work per unit time  $\triangle$  and total piston work per unit time  $\diamond$  of the SSR under isothermal conditions as a function of temperature. The working fluid is a 17% molar mixture and the period of operation is 100 s. The hot and cold piston swept volumes are  $0.76\text{ cm}^3$  and  $0.82\text{ cm}^3$ , respectively. The solid line and the long dashed line are, respectively, the calculated cooling power and the cold piston work per unit time using Eqs. 14 and 15 and Radebaugh’s tables. The short dashed line is the calculated hot piston work per unit time.

in the regenerator, the regenerator effectiveness is irrelevant. This is an important simplification, since the regenerator's performance depends strongly on poorly known quantities (for example, the details of the regenerator geometry and the thermal conductivities of the regenerator materials). Our isothermal measurements, therefore, should remove effects concerning the details of heat transfer and allow direct observation of thermodynamic properties of the working fluid.

The pressure and piston displacements are measured as functions of time by low-temperature pressure gauges and moving coil transformers, respectively. The pressure gauges (not shown) were of the Straty-Adams type,<sup>8</sup> calibrated in situ at low temperature by comparison to a room temperature diaphragm pressure gauge. The moving-coil transformers, discussed in detail elsewhere,<sup>9</sup> were checked for linearity at room temperature and calibrated at low temperature using electrical contacts at the extremes of the pistons' travel. These linear displacements were converted to volumetric displacements by multiplying the manufacturer's value for the effective area of the bellows used to seal the pistons.

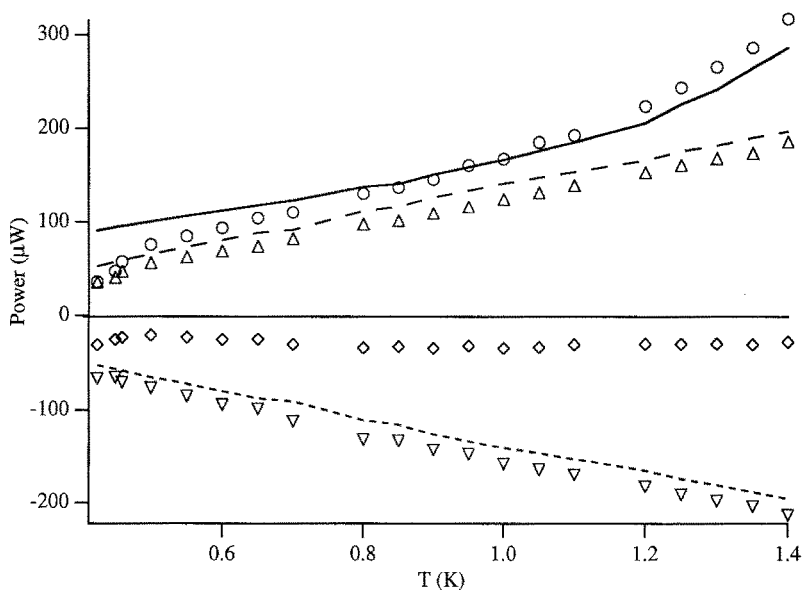


Fig. 5. Measured cooling power  $\circ$ , hot piston work per unit time  $\nabla$ , cold piston work per unit time  $\triangle$  and total piston work per unit time  $\diamond$  of the SSR under isothermal conditions as a function of temperature. The working fluid is a 17% molar mixture and the period of operation is 80 s. The hot and cold piston swept volumes are  $1.02 \text{ cm}^3$  and  $0.98 \text{ cm}^3$ , respectively. The solid line and the long dashed line are, respectively, the calculated cooling power and the cold piston work per unit time using Eqs. 14 and 15 and Radebaugh's tables. The short dashed line is the calculated hot piston work per unit time.

The pressures and displaced volumes in the SSR were recorded using an IBM AT computer. The average work done per unit time by each set of pistons is calculated from the pressure and displaced volume data using the relation

$$\dot{W} = \frac{1}{\tau} \int_0^{\tau} p dV \quad (1)$$

where  $\dot{W}$  is the average work done per unit time by the piston,  $\tau$  is an integer multiple of the period of operation of the SSR,  $p$  is the pressure, and  $dV$  is the volume displaced by the piston. The pressure relevant to the cooling action of the refrigerator is the osmotic pressure across the superleaks.

The pressure variations in each half of the SSR consist of two components. The first component does not contribute to the cooling action of the SSR: Slight asymmetries between the two SSR halves result in a time dependent fluctuation of the total volume of the SSR. In turn, this volume variation drives a large pressure fluctuation, due to the low compressibility

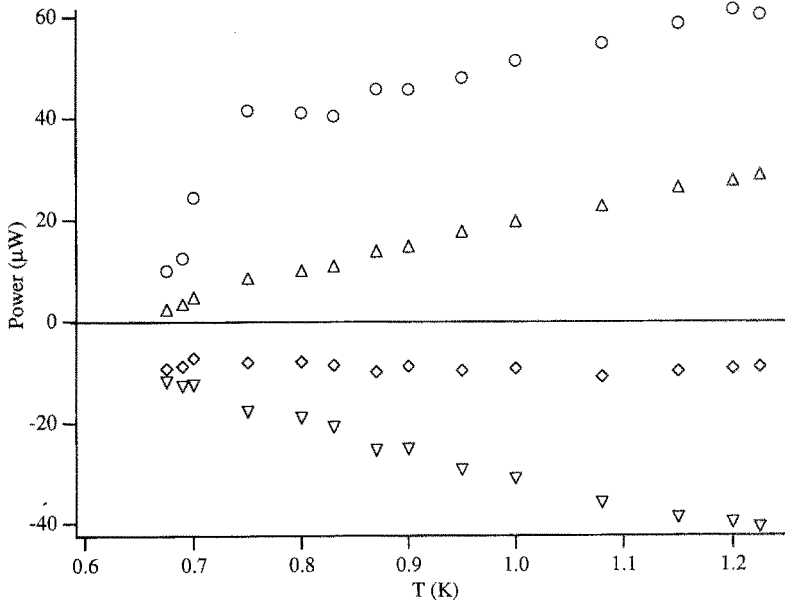


Fig. 6. Measured cooling power ○, hot piston work per unit time ▽, cold piston work per unit time △ and total piston work per unit time ◇ of the SSR under isothermal conditions as a function of temperature. The working fluid is a 36% molar mixture and the period of operation is 300 s. The hot and cold piston swept volumes are 0.76 cm<sup>3</sup> and 0.80 cm<sup>3</sup>, respectively.

of the liquid mixture, which is common to both halves of the SSR. The second pressure component is the osmotic pressure component due to the variation of  $^3\text{He}$  concentration in each half of the SSR, which is determined by measuring the pressure on each side of the superleak and taking the difference.

The operating speeds of the SSR were limited by the cooling power of the  $^3\text{He}$  evaporation refrigerator at low temperature and by a low critical velocity in the SSR at high concentration and high temperature.

Figure 3 shows the results of the isothermal operation of the SSR for a 5.9% mixture and a period of 100 s. The measured hot and cold piston works are calculated using Eq. 1. The total work is the sum of the hot and cold piston works. The cooling power is the time average (over an integral number of cycles) of the power delivered to the cold platform heater. Figures 4 and 5 are the corresponding plots for a 17% mixture for two different operating conditions and Fig. 6 is that for a 36% mixture.

### 3. IDEAL FERMI ANALYSIS

To interpret these measurements, we must realize that the  $^3\text{He}$  component of the  $^3\text{He}$ - $^4\text{He}$  mixture is expected to behave as an ideal Fermi gas at low temperatures and low concentrations. Here we develop expressions for the expected performance of the isothermal SSR if the  $^3\text{He}$  component of the working fluid behaves as an ideal Fermi gas in an inert background of superfluid  $^4\text{He}$ . Our analysis will result in expressions for the work per cycle done by the working fluid on the SSR cold piston,  $W_c$ , and the heat absorbed per cycle at the SSR cold piston by the working fluid,  $Q_c$ . We then show that the ratio  $Q_c/W_c$  is independent of the geometry of the SSR and depends only on the temperature and the thermal expansion coefficient of the working fluid. In addition, we will find that the working fluid transition from Boltzmann gas behavior to Fermi gas behavior is more apparent in the ratio  $Q_c/W_c$  than in either  $Q_c$  or  $W_c$ .

We assume that each side of the SSR can be modeled by two pistons and a regenerator of volume  $V_r$ . The volumes of the pistons vary sinusoidally as

$$V_h = V_0 + V_1 \cos \omega t \quad (2a)$$

$$V_c = V_0 - V_1 \sin \omega t \quad (2b)$$

where  $V_h$  is the "hot" piston volume (the piston where heat is rejected from the SSR),  $V_c$  is the "cold" piston volume (the piston where heat is absorbed by the SSR),  $V_0$  is the average piston volume,  $V_1$  is half the volume swept by each of the pistons,  $\omega$  is the angular frequency of operation and  $t$  is

time. The total volume in the SSR,  $V_{\text{tot}}$ , is the sum of the regenerator volume and the piston volumes or

$$V_{\text{tot}} = (2V_0 + V_r) + \sqrt{2} V_1 \cos(\omega t + \pi/4) \quad (3)$$

Since the compression in the SSR is fairly low (that is  $\sqrt{2} V_1 / (2V_0 + V_r) \ll 1$ ; in our measurements a typical value for this ratio is 0.07), the pressure in the SSR can be determined using a linearized expression with the isothermal compressibility of the working fluid  $\kappa$ :

$$p = p_{\text{ave}} + \left( \frac{\partial p}{\partial V} \right)_T (V_{\text{tot}} - V_{\text{ave}}) = p_{\text{ave}} + \frac{\sqrt{2} V_1}{\kappa(2V_0 + V_r)} \cos(\omega t + \pi/4) \quad (4)$$

where  $V_{\text{ave}}$  is the average volume in the SSR ( $=2V_0 + V_r$ ) and  $p_{\text{ave}}$  is the pressure in the SSR when the SSR volume is  $V_{\text{ave}}$ . The work done by the fluid in the cold piston,  $W_c$ , over one cycle is

$$W_c = \oint p dV_c = \frac{\pi V_1^2}{(2V_0 + V_r)} \frac{1}{\kappa} \quad (5)$$

Equation 5 shows that the work done by the working fluid on the cold piston is the product of a thermodynamic property, namely  $1/\kappa$ , and a factor that depends on the specific geometry of the SSR. Furthermore, we see from Eq. 5 that for a fixed geometry SSR the temperature dependence of the cold piston work comes only from the temperature dependence of the isothermal compressibility.

The heat absorbed by the fluid in the cold piston chamber in one cycle,  $Q_c$ , can be calculated using energy conservation:  $Q_c = W_c + H_c$ , where  $H_c$  is the total enthalpy flow over the cycle from the cold piston. Using assumptions similar to the analysis above leads to

$$H_c = -\oint h dn_c = \frac{pV_1^2}{(2V_0 + V_r)} \left( \frac{\partial h}{\partial v} \right)_T \quad (6)$$

where  $h$  is the enthalpy per mole of the working fluid,  $n_c$  is the number of moles of working fluid in the cold piston and  $v$  is the molar volume of the working fluid. With some thermodynamic manipulation, the derivative  $(\partial h / \partial v)_T$  can be shown to be  $(T\beta - 1)/\kappa$  where  $T$  is the temperature and  $\beta = (1/V)(\partial V / \partial T)_p$  is the thermal expansion coefficient. We therefore find that the heat absorbed by the cold piston per cycle is

$$Q_c = \frac{pV_1^2}{(2V_0 + V_r)} \frac{T\beta}{\kappa} \quad (7)$$

Like  $W_c$ , the heat absorbed by the cold piston is a product of a thermodynamic property, namely  $T\beta/\kappa$ , and a factor that depends on the specific geometry of the SSR. In fact, the geometric factor is the same in the expressions for  $W_c$  and  $Q_c$  (Eq. 5 and 7, respectively). The ratio of  $Q_c$  to  $W_c$  depends only on the temperature of the working fluid and the thermal expansion coefficient and does not depend on the specific geometry of the SSR. Explicitly,

$$\frac{Q_c}{W_c} = T\beta \quad (8)$$

We have shown that the isothermal compressibility, the thermal expansion coefficient, and the temperature of the working fluid affect the cold piston work, the cold piston heat absorbed and their ratio. To determine how these quantities vary for an ideal Fermi gas at temperatures and densities of the  $^3\text{He}$  used in our SSR, we use the well known expression for the pressure of an ideal Fermi gas<sup>10</sup>:

$$P = kT \frac{g}{\lambda^3} f_{5/2}(z) \quad (9)$$

where  $k$  is Boltzmann's constant,  $g$  is the spin degeneracy of the Fermi particles (equal to 2 for  $^3\text{He}$ ),  $\lambda = \sqrt{2\pi\hbar^2/(mkT)}$  is the deBroglie wavelength,  $z$  is the fugacity,  $\hbar$  is Plank's constant divided by  $2\pi$  and  $m$  is the effective mass of the  $^3\text{He}$  atom (equal to 2.45 times the rest mass of the  $^3\text{He}$  atom<sup>11, 12, 13</sup>). The function  $f_{5/2}(z)$  is defined as

$$f_{5/2}(z) \equiv \frac{4}{\sqrt{\pi}} \int_0^\infty dx x^2 \ln(1 + ze^{-x^2}) \quad (10)$$

The fugacity is determined from specific volume of the  $^3\text{He}$ ,  $v$ , and the temperature of the mixture using

$$\frac{1}{v} = \frac{g}{\lambda^3} f_{3/2}(z) \quad (11)$$

where  $f_{3/2}(z) = z(d/dz) f_{5/2}(z)$ . Using these expressions and the definition of  $\beta$ , we find

$$\beta = \frac{3}{2T} \left( \frac{5f_{5/2}(z) f_{1/2}(z)}{3(f_{3/2}(z))^2} - 1 \right) \quad (12)$$

where  $f_{1/2}(z) = z(d/dz) f_{3/2}(z)$ . Similarly, the isothermal compressibility is

$$\kappa = \frac{v}{kT} \frac{f_{1/2}(z)}{f_{3/2}(z)} \quad (13)$$

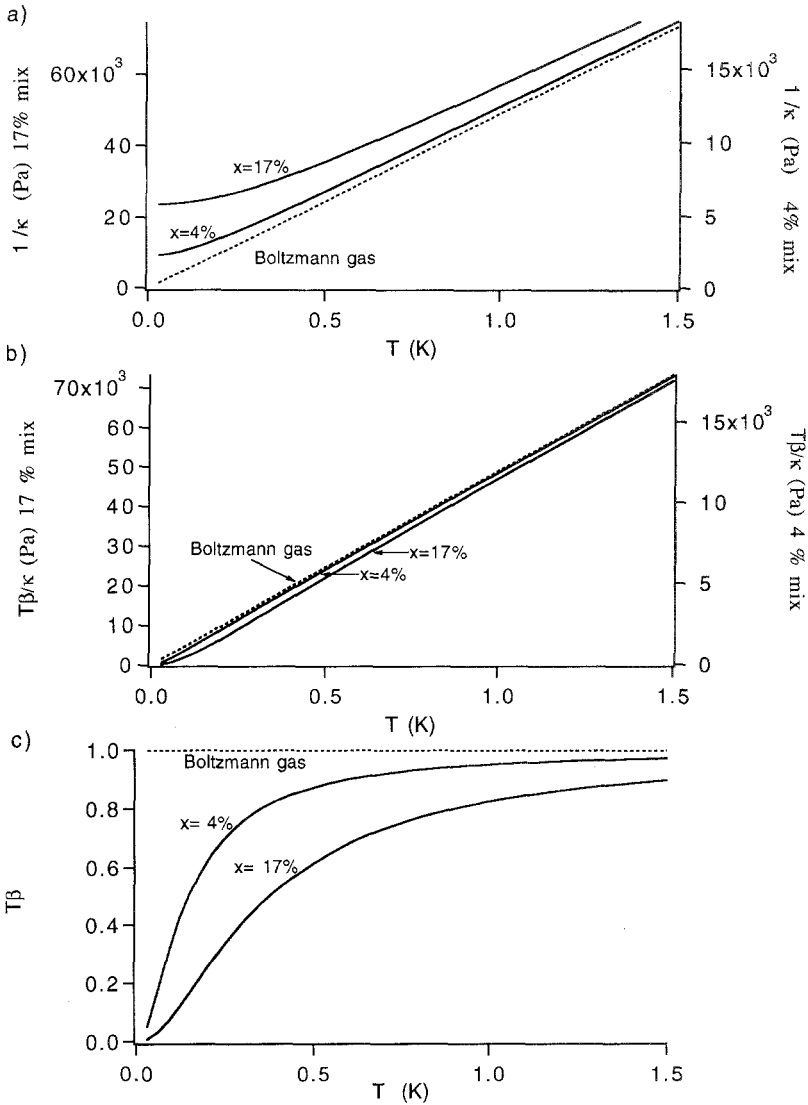


Fig. 7. Calculated Fermi gas properties are shown with solid curves. Ideal Boltzmann gas properties are shown with dotted lines. The  $x = 17\%$  curves (and correspondingly for the  $x = 4\%$  curves) are the result of a calculation using a gas density equal to that of the  $^3\text{He}$  density in a  $17\% \text{ } ^3\text{He}\text{-}^4\text{He}$  mixture. The low temperature portion of the  $17\%$  curves is experimentally unattainable in a  $^3\text{He}\text{-}^4\text{He}$  mixture due to phase separation at  $407 \text{ mK}$ . (a) Plot of the reciprocal of the isothermal compressibility of an ideal Fermi gas versus temperature. The cold piston work in the isothermal SSR is proportional to  $1/\kappa$  for the working fluid. The dotted line corresponds to the Boltzmann gas values for both  $4\%$  and  $17\% \text{ } ^3\text{He}\text{-}^4\text{He}$  concentrations. The  $4\%$  curves should be read using the right-hand scale and  $17\%$  curves should be read

Equations 12 and 13 were numerically integrated for  $^3\text{He}$  concentrations of 4% and 17% and temperatures from 0.01 K to 1.5 K. The results are shown in Fig. 7. Figure 7a is a plot of the reciprocal of the isothermal compressibility of the ideal Fermi gas versus temperature. Equation 5 shows that work done by the cold piston is proportional to this quantity. The reciprocal of the isothermal compressibility for a Fermi gas begins to deviate significantly from the linear  $T$  dependence of that of a Boltzmann gas only at very low temperature. Unfortunately, our measurements are not in this regime. In addition, the 17% mixture phase separates<sup>6</sup> at 407 mK so that the lower section of the 17% curve is unattainable in  $^3\text{He}$ - $^4\text{He}$  mixtures.

Figure 7b is a plot of  $T\beta/\kappa$  versus temperature for the ideal Fermi gas. Equation 7 shows that the cooling power of the isothermal SSR is proportional to this quantity. From the curves of Figs. 7a and 7b, we see that the Fermi effects of the  $^3\text{He}$  do not significantly alter the temperature dependence of the cooling power or the cold piston work from the linear temperature dependence of a Boltzmann gas model. However, the ratio  $Q_c/W_c$  clearly shows the Fermi nature of the working fluid. We see this in Fig. 7c which is a plot of  $T\beta$  versus temperature for the ideal Fermi gas.  $T\beta = Q_c/W_c$  by Eq. 8 and its value should approach the Boltzmann gas value of one at high temperature.  $Q_c/W_c$  should never exceed the value of unity if the working fluid behaves as an ideal Fermi gas. We will show below that our data is consistent with the ideal Fermi gas only at low concentration and low temperature.

The ideal-Fermi-gas picture can be extended analytically,<sup>14</sup> in powers of the excitation-spectrum wave number, to compute these properties for a *nearly* ideal Fermi gas. The corrections to the ideal calculations are small; for example, for the 17% mixture, the nearly ideal calculation increases  $T\beta$  by only 0.01 between 0.5 K and 1 K.

We would like to emphasize here that the quantities above are properties ascribed to the  $^3\text{He}$  component of the mixture and not to the  $^3\text{He}$ - $^4\text{He}$  mixture itself. These quantities are osmotic values,<sup>15</sup> consistent with our assumption that the  $^4\text{He}$  component of the mixture is inert (and that the chemical potential of the  $^4\text{He}$  is constant) throughout the Stirling process. In this section, we have assumed that the essential physics is captured by considering only the participation of the  $^3\text{He}$  component in the cycle.

---

using the left-hand scale. (b) Plot of  $T\beta/\kappa$  versus temperature. The cooling power in the isothermal SSR is proportional to  $T\beta/\kappa$  for the working fluid. The dotted line corresponds to the Boltzmann gas values for both 4% and 17%  $^3\text{He}$ - $^4\text{He}$  concentrations. The 4% curves should be read using the right-hand scale and 17% curves should be read using the left-hand scale. (c) Plot of  $T\beta$  versus temperature. Note that for ideal Boltzmann gas,  $T\beta$  has a constant value of 1. The ratio of the isothermal SSR cooling power divided by the cold piston work is equal to  $T\beta$  for the working fluid.

#### 4. GENERAL THERMODYNAMIC ANALYSIS

Brisson and Swift<sup>4</sup> (B & S) measured and analyzed the isothermal operation of the SSR for high temperatures ( $T > 1$  K) and showed that the  $^4\text{He}$  component of the mixture did not behave as an inert background but significantly augmented the SSR cooling power at uniform temperature. The excitations in the  $^4\text{He}$  (the phonons and rotons) contribute to the high temperature cooling power of the SSR above that due to the  $^3\text{He}$  component. They developed expressions that are relevant to the measurements we describe here. Their result for the work done per cycle by the working fluid on the cold piston,  $W_c$ , is

$$W_c = \frac{1}{\rho} \left( \frac{\partial p}{\partial c} \right)_{T, \mu_4} \frac{\pi M_3 V_1^2}{(2V_0 + V_r)^2} \quad (14)$$

where  $\rho$  is the mixture's total mass density,  $T$  is the temperature,  $p$  is the pressure,  $M_3$  is the total mass of  $^3\text{He}$  on one side of the SSR,  $c$  is the mass concentration of the mixture,  $\mu_4$  is the chemical potential of the  $^4\text{He}$ . The heat absorbed per cycle by an isothermal SSR,  $Q_c$ , is

$$Q_c = \left[ \frac{1}{\rho} \left( \frac{\partial p}{\partial c} \right)_{T, \mu_4} - c_0 \left( \frac{\partial h_{os}}{\partial c} \right)_{T, \mu_4} \right] \frac{\pi M_3 V_1^2}{(2V_0 + V_r)^2} \quad (15)$$

where  $h_{os}$  is the osmotic enthalpy and  $c_0$  is the average  $^3\text{He}$  mass concentration. They find the ratio of the heat absorbed per cycle divided by the cold piston work is

$$\frac{Q_c}{W_c} \approx -\rho c_0 \frac{(\partial h_{os}/\partial c)_{T,p}}{(\partial p_{os}/\partial c)_{T,p}} - \rho(1 - c_0) \frac{(\partial \mu_4/\partial c)_{T,p}}{(\partial p_{os}/\partial c)_{T,p}} \quad (16)$$

where  $p_{os}$  is the osmotic pressure. Note that their result for  $Q_c/W_c$  depends only on working fluid properties and not on the specific geometry of the SSR, in agreement with the conclusion reached in Sec. 3. Equations 14–16 can be evaluated using thermodynamic tables.<sup>6</sup>

#### 5. COMPARISON WITH MEASUREMENTS

In reality, operation of the actual SSR is not isothermal and so we expect that the geometric factors present in Eqs. 5, 7, 14 and 15 are effectively too small if we use the isothermal compressibility  $\kappa$  in these equations. We compensate for this by following B & S's approach of introducing

an effective mean fluid volume,  $V_{\text{eff}}$ , to replace the average volume,  $V_{\text{ave}} = 2V_0 + V_r$ , in these equations. For a monatomic Boltzmann gas, the isothermal compressibility is 5/3 times larger than the adiabatic compressibility, so fluid experiencing adiabatic processes would have an effective volume only 3/5 of its actual volume. Fluid near the wall experiences nearly isothermal processes; whereas, fluid far from the wall experiences nearly adiabatic processes. The thermal penetration depth, which is the characteristic distance from the walls separating these two extremes, depends on frequency, temperature and concentration. For example, with an operating frequency of 0.01 Hz the penetration depth is 5 mm at 0.4 K and a  $^3\text{He}$  concentration of 6.5%. The penetration depth decreases to 3 mm at a temperature of 1 K and a concentration of 18%. As a result, the effective volume of the refrigerator is a function of frequency, temperature and concentration.

Following B & S, we determine the effective mean volume,  $V_{\text{eff}}$ , by examining the osmotic pressure oscillations. With piston motions given by Eq. 2, the osmotic pressure difference between the two halves of the SSR is

$$\Delta p_{\text{os}}(t) = \frac{M_3}{\rho} \left( \frac{\partial p}{\partial c} \right)_{T, \mu_4} \left\{ [V_{\text{eff}} + \sqrt{2} V_1 \cos(\omega t + \pi/4)]^{-1} - [V_{\text{eff}} - \sqrt{2} V_1 \cos(\omega t + \pi/4)]^{-1} \right\} \quad (17)$$

Each term in the square brackets corresponds to each half of the SSR. The maximum and minimum osmotic pressure difference between the SSRs ( $p_{\text{max}}, p_{\text{min}}$ ) is easily measured from the data. Since the maximum and minimum pressures for Eq. 17 occur when  $\omega t = 3\pi/4$  and  $7\pi/4$ , we find that

$$V_{\text{eff}} = \left[ \frac{M_3}{\rho} \left( \frac{\partial p}{\partial c} \right)_{T, \mu_4} \frac{4\sqrt{2} V_1}{p_{\text{max}} - p_{\text{min}}} + 2V_1^2 \right]^{1/2} \quad (18)$$

The derivative  $(\partial p/\partial c)_{T, \mu_4}$  is evaluated using Radebaugh's tables. Figure 8 contains plots of the effective volume as a function of temperature using the 5.9% and 17% SSR data, Radebaugh's tables and Eq. 18. If the operation of the SSR were isothermal then the effective volume would equal the SSR's mean volume of  $7.3 \text{ cm}^3$ , shown as the upper dotted line in Fig. 8. The adiabatic limit of  $V_{\text{eff}}$ , for a monatomic ideal gas, is 3/5 the isothermal limit volume and is shown as the lower dashed line.

The 5.9% effective volume results show a broad maximum in  $V_{\text{eff}}$  which corresponds to near isothermal operation. The reduction in  $V_{\text{eff}}$  at

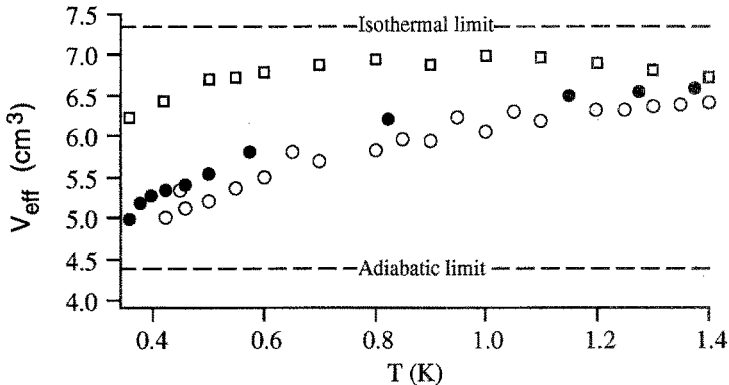


Fig. 8. The effective volume, calculated using Eq. 18, as a function of uniform SSR temperature:  $\square$  corresponds to the 5.9% molar mixture measurements of Fig. 3;  $\bullet$  corresponds to the low frequency, short piston stroke measurements of Fig. 4 (17% molar mixture, 100 s period);  $\circ$  corresponds to the high frequency, long piston stroke measurements of Fig. 5 (17% molar mixture, 80 s period).

low temperature is due to the increased Kapitza resistance, which thermally decouples the mixture from its surroundings so that the expansions and compressions are more adiabatic. The reduction of the effective volume at high temperature can be attributed to the increased heat capacity per unit volume of the fluid mixture, due to the creation of phonons and rotons in the  $^4\text{He}$  component, which reduces the thermal penetration depth so that more of the fluid behaves adiabatically. The 17% mixture results shows no such reduction at high temperature, because the contribution of the  $^4\text{He}$  component's phonons and rotons to the heat capacity is dominated by the contribution of the  $^3\text{He}$  component. The 17% results also show a frequency dependence due to the frequency dependence of the thermal penetration depth.

We use these values for  $V_{\text{eff}}$  to compare measured works and heats to the values predicted by the B & S model. The expected cold piston work and cooling power are calculated using Eq. 14 and Eq. 15, respectively, by substituting  $V_{\text{eff}}$  for  $2V_o + V_r$ . The results of these calculations are shown in Figs. 3, 4 and 5 with solid and dashed lines. The long dash lines correspond to the cold piston work and the short dashed lines correspond to the hot piston work (which is equal and opposite to the cold piston work). The solid line corresponds to the model's cooling power for the SSR.

The effective volume used in our analysis is derived from the measured osmotic pressure oscillations in the SSR. Since the work is the integral of  $p dV$ , it is not surprising that the work calculated with the B & S model fits the work data so well in Figs. 3–5. Both the hot and cold piston work

linearly decrease with temperature for all temperatures and concentrations measured. This linear temperature dependence of the piston work is consistent with the Boltzmann gas model, the Fermi gas model (see Fig. 7a), and the B & S model for the temperature and concentrations measured. For a reversible cycle at uniform temperature, we would expect that the total piston work (the cold piston work plus the hot piston work  $\equiv W_{\text{tot}}$ ) would be zero. Figures 3–6 indicate that the operation of the SSR is irreversible since the total work is nonzero and negative. This is also supported by the effective volume measurements since they indicate that the SSR's operation is neither entirely isothermal nor entirely adiabatic.

The cooling power of the SSR is not linear with temperature. Figures 3–5 (especially Fig. 3) show the augmented high temperature cooling power due to phonons and rotons in the  $^4\text{He}$  component of the mixture, previously described by Brisson and Swift.<sup>4</sup> Figures 4 and 5 show that below about 0.5 K the cooling power drops well below the value predicted by the B & S model.

We have not plotted the B & S model in Fig. 6 since the Radebaugh's tables do not extend to the 36% mixture concentration used there. The high temperature phonon-roton cooling power increase is not apparent in our 36% mixture measurements and the low temperature cooling power drops precipitously below 0.75 K.

Above, we showed that the ratio of  $Q_c/W_c$  is geometry independent and hence is a good check of the working fluid models, indicating the useful range of these models. Our derivations assumed isothermal and reversible operation of the SSR; unfortunately, our data show that the SSR is not isothermal or reversible ( $V_{\text{eff}} \neq 2V_0 + V_r$  and  $W_{\text{tot}} \neq 0$ ). In addition, our derivations assumed that there was no heat leak to the cold piston platform. In an attempt to account for these small effects, we calculate from the data the ratio

$$\frac{Q_{c, \text{rev}}}{W_{c, \text{rev}}} \equiv \frac{Q_{c, \text{meas}} + Q_{c, \text{bkgd}} + |W_{\text{tot}}/2|}{W_{c, \text{meas}} + |W_{\text{tot}}/2|} \quad (19)$$

where  $Q_{c, \text{rev}}$  is the reversible heat absorbed by the cold piston per cycle,  $Q_{c, \text{meas}}$  is the actual heat absorbed by the cold piston per cycle, and  $Q_{c, \text{bkgd}}$  is the background heat to the cold piston per cycle.  $W_{c, \text{rev}}$  and  $W_{c, \text{meas}}$  are the reversible work and the measured work done by the cold piston per cycle.  $W_{\text{tot}}$  is the total energy dissipated per cycle ( $W_{\text{tot}}$  is equal to the sum of the cold piston work per cycle and the hot piston work per cycle). In developing Eq. 19, we assume that half of  $W_{\text{tot}}$  is dissipated in the cold piston and the other half is dissipated in the hot piston. The net effect is a reduction in the actual cooling power,  $Q_{c, \text{meas}}$ , from the ideal cooling

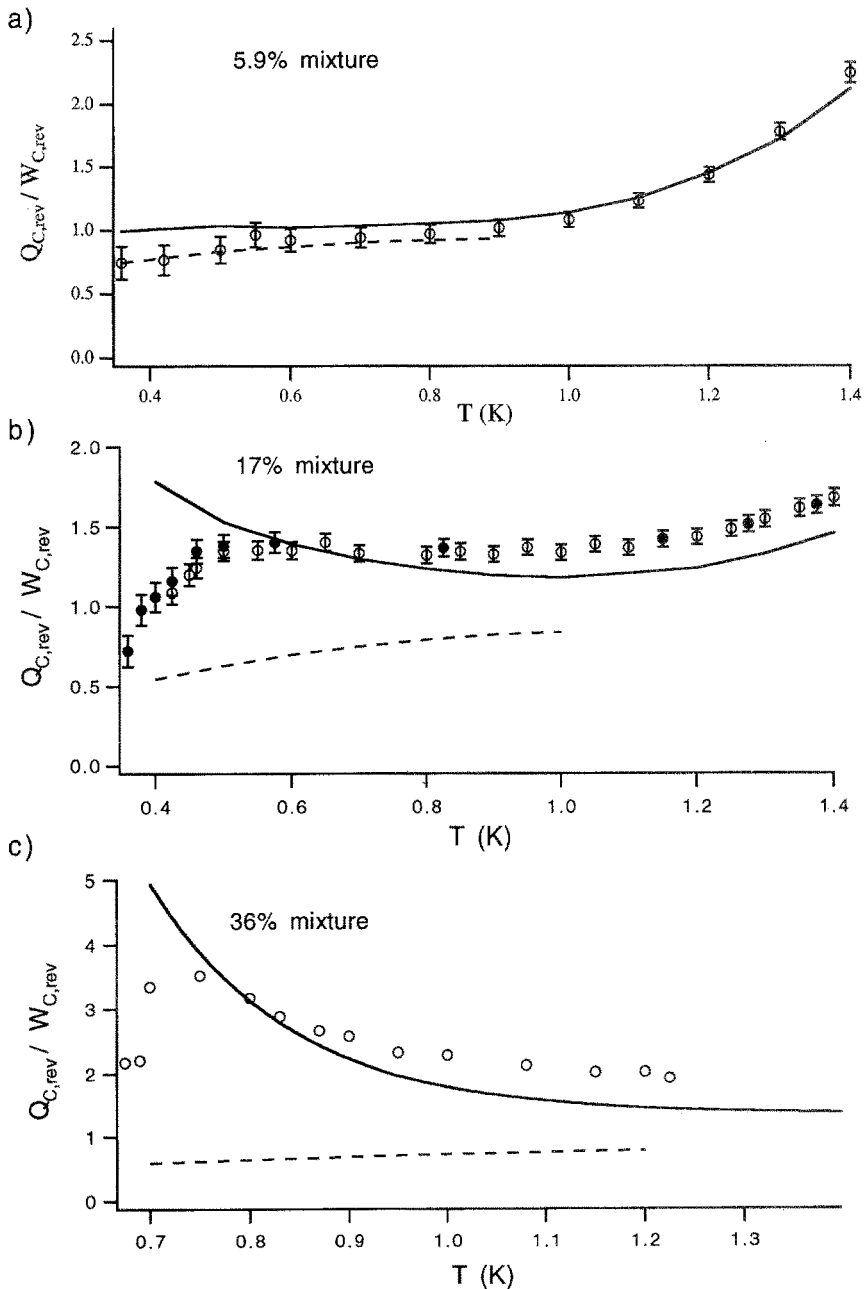


Fig. 9. The ratio of reversible cooling power to reversible mechanical power extracted by the cold piston versus temperature. The circular symbols are calculated from Eq. 19 using

power,  $Q_{c, \text{rev}}$ , by  $|W_{\text{tot}}/2|$ . The background heat,  $Q_{c, \text{bgd}}$ , primarily due to dissipation in flexing the bellows, is small and has a time averaged value of about  $2 \pm 1 \mu\text{W}$  for our measurements.

The ratio  $Q_{c, \text{rev}}/W_{c, \text{rev}}$ , calculated directly from the data, appears in Fig. 9a–c. In each of these figures, the values of  $Q_c/W_c$  for the ideal Fermi gas model (dashed line) and the B & S model (solid line) are also plotted. The overall agreement between the measurements and the B & S model shown in Fig. 9 is the principal result of this work.

Figure 9a shows that for the 5.9% concentration mixture both the B & S model and the ideal Fermi gas model agree with the measured values. The ideal Fermi gas model is only plotted for temperatures below 0.9 K since this model does not include the effect of the  $^4\text{He}$  phonon and roton excitations present above 1 K.

Figure 9b shows that for high concentration mixtures  $Q_c/W_c$  is significantly larger than what is expected using the ideal Fermi gas model (note that most of the  $Q_c/W_c$  data are greater than 1, the largest possible value for the ideal Fermi gas model). Using Radebaugh's table, the B & S model predicts an increasing  $Q_c/W_c$  ratio as the temperature is lowered. We do not see this effect in the 17% experimental results before the  $Q_c/W_c$  ratio drops as the mixture approaches phase separation. In addition, the B & S model using Radebaugh's tables underestimates the measured values of  $Q_c/W_c$  by about 20% for the high temperature 17% mixture data.

The 36% mixture experimental results in Fig. 9c show the rise in  $Q_c/W_c$  as the temperature is lowered. The solid curve depicting the B & S model is based on extrapolated values of Radebaugh's tables since these tables extend only to 30%  $^3\text{He}$  concentrations. Despite the large uncertainty due to this extrapolation, the B & S model shows the same trends as the experimental results, although it continues to underestimate  $Q_c/W_c$  at high temperature. The  $Q_c/W_c$  ratio is larger than predicted by the ideal Fermi gas model by roughly a factor of two.

In both Fig. 9b and 9c the value of  $Q_c/W_c$  drops precipitously as the phase separation temperature is approached. This drop in the value of  $Q_c/W_c$  occurs before the SSR mixture phase separates. (Figure 10 shows the operating conditions discussed in this paper superimposed on a  $^3\text{He}$ - $^4\text{He}$

---

measured values. The error bars correspond to experimental uncertainty in the background heat load to the cold piston,  $Q_{c, \text{bgd}}$ . The solid lines are the  $T\beta$  values for the B & S model and the dashed lines are the  $T\beta$  values for an ideal Fermi gas. (a) Values for a 5.9% mixture. The Fermi temperature for this concentration is 0.34 K. (b) Values for a 17% mixture. The filled and unfilled symbols correspond to the measurements of Figs. 4 and 5, respectively. The Fermi temperature for this mixture is 0.74 K. (c) Values for the 36% measurements. The Fermi temperature for this concentration is 1.19 K.

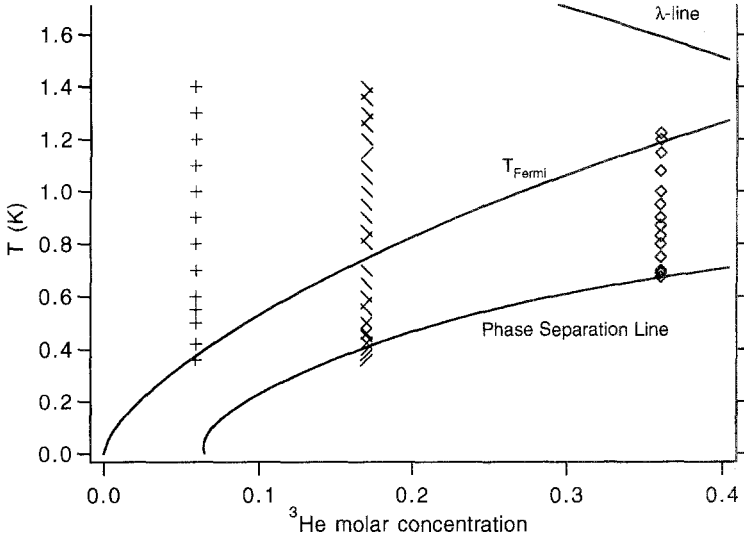


Fig. 10. Plot of the concentrations versus temperature for the measured operating points described in this paper. The phase separation line,  $\lambda$ -line and the Fermi temperature as a function of  $^3\text{He}$  concentration are also plotted. The symbols +, \, / and  $\diamond$  correspond to the mixture concentrations and period of operation 5.9% and 100 s, 17% and 17% and 80 s, 17% and 100 s, 36% and 300 s, respectively.

diagram.) We believe that this effect may be due to a reduced critical velocity in the  $^3\text{He}$ - $^4\text{He}$  mixture as the phase separation curve is approached. Zeegers *et al.*<sup>16</sup> found an empirical relation for the critical velocity of a saturated helium mixture in a capillary below 100 mK:

$$v_c = \frac{K}{d} \ln \left( \frac{d}{d_0} \right) \quad (20)$$

where  $K = 0.05 \text{ cm}^2/\text{s}$ ,  $d$  is the diameter of the capillary, and  $d_0 = 15 \mu\text{m}$ . Zeegers' relation does not necessarily apply at the high temperatures and concentrations we have in our measurements; however, we are unaware of any more relevant measurements of critical velocity. The maximum velocity in the 0.8 mm diameter channel between the piston chamber and the heat exchanger is 4.3 cm/s which exceeds the corresponding Zeegers critical velocity of 2.5 cm/s. We believe this channel to be the critical limitation in our current SSR's performance at high concentration. Future SSRs can be designed to operate with such a high concentration mixture by using many small diameter passages. The smaller diameters increase the critical velocity (see Eq. 20) while the increased number of passages reduces the flow velocity in each passage.

In conclusion, we note that the Fermi model is appropriate for low temperature and low concentration mixtures. However, thermodynamic tables are necessary to predict high concentration SSR performance. Unfortunately, these tables<sup>6</sup> extend only to concentrations of 30%. In addition, there is a need for more accurate fundamental thermodynamic data at all concentrations, to generate more accurate thermodynamic tables.

### ACKNOWLEDGMENTS

This work was supported by the Office of Basic Energy Sciences in the US Department of Energy and by the National Science Foundation.

### REFERENCES

1. J. Wilks. *The Properties of Liquid and Solid Helium*, Clarendon, Oxford (1967), p. 232.
2. V. Kotsubo and G. W. Swift, "Superfluid Stirling refrigerator: a new method for cooling below 1 Kelvin," in *Proceedings of the Sixth International Cryocoolers Conference*, Geoffrey Green and Margaret Knox, ed., David Taylor Research Center, Bethesda, Md (1991).
3. V. Kotsubo and G. W. Swift, "Superfluid Stirling-cycle refrigerator below 1 Kelvin," *J. Low Temp. Phys.* **83**, 217 (1991).
4. J. G. Brisson and G. W. Swift, "High-temperature cooling power of the superfluid Stirling refrigerator," *J. Low Temp. Phys.* **98**, 141 (1995).
5. A. Watanabe, G. W. Swift, and J. G. Brisson, "Measurements with a Recuperative Superfluid Stirling Refrigerator;" To be published in *Advances in Cryogenic Engineering* **41**, 1996.
6. R. Radebaugh, "Thermodynamic properties of  $^3\text{He}$ - $^4\text{He}$  solutions with applications to the  $^3\text{He}$ - $^4\text{He}$  dilution refrigerator," NBS Tech Note 362 (1967).
7. Type 30 bellows, Senior Flexonics Inc., Metal Bellows Division, 1075 Providence Highway, Sharon, MA 02067.
8. G. C. Straty and E. D. Adams, "Highly sensitive capacitive pressure gauge," *Rev. Sci. Instrum.* **40**, 1393 (1969).
9. J. G. Brisson and G. W. Swift, "Superfluid Stirling refrigerator with a counterflow regenerator," in *Proceedings of the Seventh Cryocooler Conference*, Phillips Laboratory, Kirtland AFB, NM (1993), 460.
10. See for example: K. Huang, *Statistical Mechanics*, John Wiley & Sons, New York (1963), p. 200.
11. D. O. Edwards, D. F. Brewer, P. Seligman, M. Skertic and Yakub, *Phys. Rev. Lett.* **15**, 773 (1965).
12. A. C. Anderson, D. O. Edwards, W. R. Roach, R. E. Sarwinski, and J. C. Wheatley, *Phys. Rev. Lett.* **17**, 365 (1966).
13. A. C. Anderson, W. R. Roach, R. E. Sarwinski, and J. C. Wheatley, *Phys. Rev. Lett.* **16**, 263 (1966).
14. A. Th. A. M. de Waele and J. G. M. Kuerten, "Thermodynamics and hydrodynamics of  $^3\text{He}$ - $^4\text{He}$  mixtures," *Progress in Low Temp. Phys.* **13**, 167 (1992).
15. See for example: E. A. Guggenheim, *Thermodynamics, An Advanced Treatment for Chemists and Physicists*, 4th ed. (North Holland, Amsterdam, 1959), Chaps. 5 and 6.
16. J. C. H. Zeegers, R. G. K. M. Aarts, A.T.A.M. de Waele, and H. M. Gijnsman, "Critical velocities in  $^3\text{He}$ - $^4\text{He}$  mixtures below 100 mK," *Phys. Rev. B* **45**, 12442 (1992).